nature astronomy

LETTERS

https://doi.org/10.1038/s41550-018-0453-9

The mysterious age invariance of the planetary nebula luminosity function bright cut-off

K. Gesicki[1*], A. A. Zijlstra[2,3] and M. M. Miller Bertolami[4]

Planetary nebulae mark the end of the active life of 90% of all stars. They trace the transition from a red giant to a degenerate white dwarf. Stellar models[1,2] predicted that only stars above approximately twice the solar mass could form a bright nebula. But the ubiquitous presence of bright planetary nebulae in old stellar populations, such as elliptical galaxies, contradicts this: such high-mass stars are not present in old systems. The planetary nebula luminosity function, and especially its bright cut-off, is almost invariant between young spiral galaxies, with high-mass stars, and old elliptical galaxies, with only low-mass stars. Here, we show that new evolutionary tracks of low-mass stars are capable of explaining in a simple manner this decades-old mystery. The agreement between the observed luminosity function and computed stellar evolution validates the latest theoretical modelling. With these models, the planetary nebula luminosity function provides a powerful diagnostic to derive star formation histories of intermediate-age stars. The new models predict that the Sun at the end of its life will also form a planetary nebula, but it will be faint.

Low and intermediate-mass stars, up to about 8 solar masses ($M_\odot$), end their lives with a phase of extreme mass loss. The superwind ejects the envelope, leaving only the degenerate core behind. The core briefly ionizes the ejecta before entering the terminal white-dwarf cooling stage. The ionized ejecta remain visible as a planetary nebula (PN) for thousands of years, before dispersing into the interstellar medium[3].

Planetary nebulae form the most luminous phase of evolution of their host stars, with typical luminosity $L \approx 10^4$ solar luminosities, $L_\odot$. In addition, much of the nebular luminosity comes out in a few bright, narrow emission lines. The brightest line, [O III] 5,007 Å, can emit as much as $10^3 L_\odot$. This makes PNe detectable to very large distances, including galaxies beyond the Virgo cluster. The planetary nebula luminosity function (PNLF) has been established as an important extragalactic distance estimator[4,5]. However, stellar evolution models have thus far been unable to explain it[6].

The PNLF describes the fraction of PNe in a galaxy at each specified luminosity bin[7]. For the emission line [O III] 5,007 Å, the absolute magnitude is defined[8] as $M_{5007} = -2.5 \log(F[\mathrm{O\,III}]) - 13.74$. Here $F([\mathrm{O\,III}])$ is the line flux in units of erg s^{-1} cm^{-2}, assuming a distance of 10 pc. In these units, the PNLF shows a well-defined, steep cut-off at the bright end, at $M^*_{5007} \approx -4.5$. The observed value of M^*_{5007} is almost invariant between different galaxies, with a scatter of only ~0.17 mag (ref. [5]) for metal-rich galaxies. The observed magnitudes include the effect of extinction within the circumstellar material of the PN, which especially for very young and compact PNe can be of the order ~0.5 mag (see the Supplementary Discussion).

To reproduce the invariant cut-off, some studies[9] assumed a final stellar mass distribution with an upper cut-off at $0.63 M_\odot$ (initial mass $M_\mathrm{i} \approx 2 M_\odot$). This is much too high for older stellar populations[10]. Other studies[11,12] showed that the stellar evolution models available before 2016[1,2], combined with nebular models of evolving optical thickness, predicted a brightening of M^*_{5007} by more than four magnitudes when going from old (10 Gyr) to young (1 Gyr) stellar populations, in stark contradiction to the observed invariance of M^*_{5007}. These inconsistencies are a long-standing mystery in the study of the PNLF and have thrown doubts on our understanding of the final evolution of low-mass stars, including the Sun.

Recently, the details of the stellar evolution models[1,2] applied in the modelling of the PNLF have been questioned. The analysis of PNe in the Galactic bulge[13] suggested that the speed of the stellar evolution during the PN phase had been underestimated by a factor of three or more. Independently, new stellar evolution models for post-asymptotic giant branch (post-AGB) stars were developed[14], with a carefully computed post-AGB phase based on new opacities, an updated treatment of the stellar physics and a proper account of previous evolutionary stages (see Fig. 1). These new models have very different initial–final mass relations calibrated to be in good agreement with observations. Their post-AGB evolution is faster and brighter than the previous models. The new models fundamentally change the interpretation of the PNLF.

From this new model grid, we selected seven evolutionary sequences with metallicity $Z = 0.01$, representative of a wide range of solar-like populations. The initial masses range from $1 M_\odot$ to $3 M_\odot$ and the final masses from $0.532 M_\odot$ to $0.706 M_\odot$ respectively. This initial mass range corresponds to stellar ages between 0.5 Gyr and 10 Gyr (see the inset in Fig. 1). The grid includes previously published sequences[14] and newly computed models using the same physical assumptions.

The evolutionary sequence provides the temperature evolution and the luminosity evolution of the post-AGB star. To model the PNLF, we calculated emission line fluxes of model nebulae surrounding each one of the stellar models. The complete photoionization structures of the nebulae were calculated using the Torun codes[15], to derive the flux of the single nebular line used, [O III] 5,007 Å.

We first ran models with a non-evolving constant density shell, with a fixed inner radius of 0.01 pc, outer radius of 0.02 pc and mass of $0.15 M_\odot$. These parameters were chosen to result in ionization-bounded (opaque) nebulae and were adopted for each of the seven evolutionary sequences. In this maximum-nebula hypothesis, the fluxes emitted at each phase of the stellar evolution are maximized. This is appropriate for testing whether these PNe can reproduce the peak of the PNLF.

[1]Centre for Astronomy, Faculty of Physics, Astronomy and Informatics, Nicolaus Copernicus University, Torun, Poland. [2]Jodrell Bank Centre for Astrophysics, School of Physics & Astronomy, University of Manchester, Manchester, UK. [3]Department of Physics & Laboratory for Space Research, University of Hong Kong, Lung Fu Shan, Hong Kong. [4]Instituto de Astrofísica de La Plata, UNLP-CONICET, La Plata, Argentina. *e-mail: kmgesicki@umk.pl

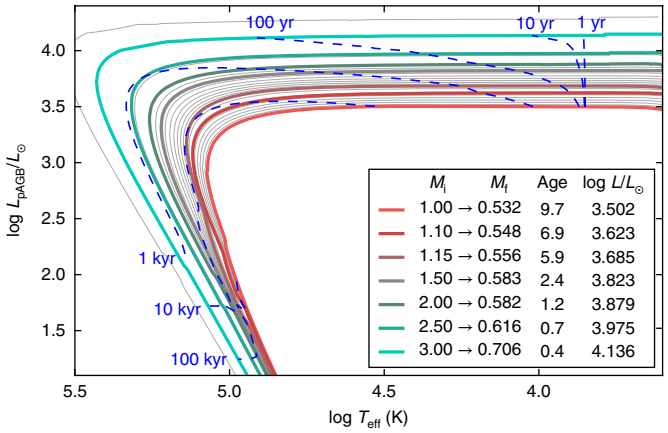

Fig. 1 | Stellar evolution sequences and timescales. The coloured lines present the post-AGB stellar evolution sequences[14] adopted for the computations of the fluxes shown in Fig. 2. Blue dashed lines indicate isochrones at selected post-AGB ages. Thin grey lines show the interpolated sequences used for the construction of the PNLFs shown in Fig. 3. The inset presents the model parameters for the seven computed tracks: the initial and final masses in $M_\odot$ units, the total age since zero-age Main Sequence in Gyr and the log $L/L_\odot$.

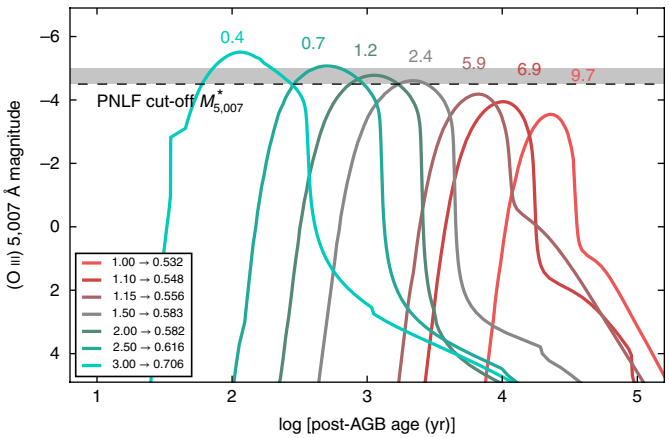

Fig. 2 | Evolution of [O III] 5007 Å fluxes against logarithmic time for the maximum-nebula hypothesis. The solid lines represent evolutionary tracks of central stars, with initial and final masses as given in the inset in units of $M_\odot$. The numbers above each curve indicate the total age in Gyr of a given stellar model. The PNLF canonical cut-off value of $M_{5007} = -4.5$ mag is shown as a horizontal dashed line; the grey band represents the possible range of this value when correction for extinction is considered (see Supplementary Fig. 1).

For each evolutionary sequence, we computed the fluxes emitted in the line [O III] 5,007 Å, converted to the magnitude scale M_{5007}. Figure 2 shows this magnitude evolution during the post-AGB evolution for the seven low-mass stars introduced in Fig. 1. The most massive track reaches magnitudes above the observed PNLF cut-off value. However, the time spent at maximum brightness is negligible in comparison with the average lifetime of PNe: the typical observed kinematic age of PNe is between ~1,000 yr and 10,000 yr. In addition, the high-mass, youngest PNe are expected to be more compact and may have considerable circumstellar extinction. The next five less-massive tracks behave very regularly, and over thousands of years they show an [O III] brightness very close to the observed cut-off value, exceeding it (if at all) by only a fraction of a magnitude. This is a consequence of the very similar post-AGB luminosity of these models (see the inset in Fig. 1) which changes by only 0.25 dex between the $1.1M_\odot$ and the $2M_\odot$ sequences (ages 7 Gyr and 1 Gyr respectively). Finally, the least massive track, at $1M_\odot$, evolves so slowly that the ejected nebula will be dispersed before the star culminates in effective temperature T_{eff}. The new stellar evolution models coupled with photoionization modelling under the maximum-nebula hypothesis predict the maximum nebular [O III] brightness to be close to the observed value over a large range of stellar ages and masses (Fig. 2). This already suggests that the models can reproduce the PNLF cut-off for a variety of stellar populations.

Next, we allow the modelled gaseous shell to evolve together with the central star. We again assume a constant density shell with fixed inner radius of 0.01 pc and fixed total mass of 0.10 $M_\odot$, but now the outer radius expands from 0.02 pc up to 0.5 pc at a constant velocity. The expansion of the shell results in a transition of the nebula from opaque to transparent to the ionizing radiation. Varying the kinematics provides different [O III] brightness scenarios. In the following, we will discuss two such scenarios: one in which the PN is predominantly opaque during the stellar evolution (the intermediate-nebula hypothesis) and the other in which the PN is predominantly transparent (the minimum-nebula hypothesis).

To derive the PNLF, we integrate over the stellar mass distribution, assuming a Salpeter initial mass function (IMF) with $n(M) \propto \mathrm{d}M \times M^{-2.35}$. We interpolate between the stellar models (Fig. 1) to get a grid of tracks at equally spaced ages. Figure 3 combines the models to predict PNLFs for both the intermediate- and minimum-nebulae hypotheses, and for four different star formation histories (SFHs), appropriate to different galaxy types. The filled histograms (dark for the intermediate-nebula hypothesis with mostly opaque PNe, pale for the minimum-nebula hypothesis with more transparent PNe) use a constant SFH, approximating a non-interacting spiral galaxy. The other two diagrams (shown with coloured lines) use a truncated SFH in which a constant star formation ceased 3, 6 and 9 Gyr ago, typical for an elliptical galaxy and for an old stellar population, formed in a burst about 9 Gyr ago.

For the intermediate-nebula hypothesis (the two upper panels in Fig. 3), the steep bright-end cut-off of the PNLF appears in our simulations for both the continuous and truncated SFHs, at a value very close to the canonical observed limit of $M^*_{5007} \approx -4.5$. The brightest PNe are created by progenitors $1.1M_\odot < M_i < 2M_\odot$, which have nearly the same post-AGB stellar luminosity, $\log(L_{pAGB}/L_\odot) = 3.75 \pm 0.13$, and have total ages from 1 to ~7 Gyr. The initial stellar masses are considerably smaller than was required in similar older models. The fact that the cut-off appears at the right magnitude over a wide age range of stellar populations provides a simple solution to the long-standing mystery of the observed invariance of the PNLF cut-off.

The two lower panels in Fig. 3 present the minimum-nebula hypothesis. This reproduces the observed faint-tail behaviour of PNLF, but the bright end becomes progressively fainter with age of the population.

We conclude that the PNLF can be reproduced using the new stellar models, under the assumptions that the ejected shells can be approximated with the intermediate-nebula hypothesis, and that the originating stellar population harbours a considerable number of stars with ages of 3–7 Gyr. The age range is consistent with the known SFH, in which nearby galaxies with masses between $10^{10}M_\odot$ and $10^{11}M_\odot$ tend to have declining star formation rates since 3–5 Gyr ago[16]. Elliptical galaxies can also contain a fraction of stars in this age range[17]. Our results confirm previous studies[18] that concluded that appropriate PNLF peak luminosities could be attained by lower-mass stars if the nebulae remained optically thick during most of their evolution.

The necessary condition that the modelled spherical PNe remain opaque during a considerable part of their early evolution can perhaps be satisfied by a high opacity in one direction and transparency in another. For bipolar PNe containing a dense equatorial

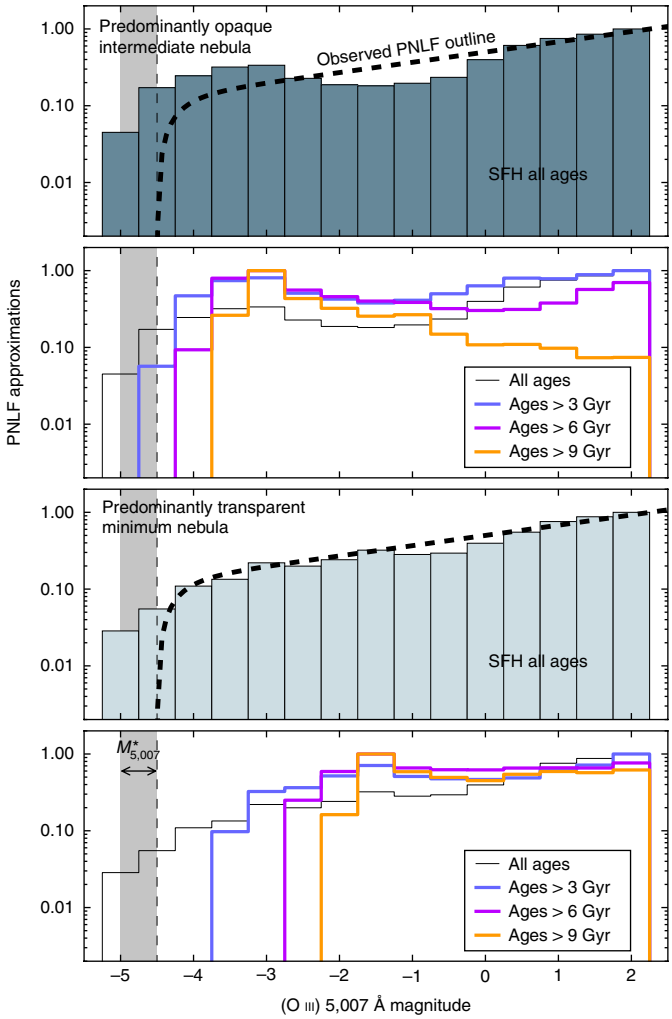

Fig. 3 | The synthesized PNLF for the intermediate-nebula and minimum-nebula hypothesis, for different SFHs. We interpolated between evolutionary tracks (Fig. 1) to obtain a grid of models sampled at uniform age. For each assumed SFH, we summed up the individual PNLFs from each gridded model, with weighting factors determined by the SFH, combined with the mass difference between adjacent interpolated tracks, and assuming a Salpeter initial mass function. The PNLF synthesis was performed for two versions of a very simple nebular evolution scenarios. The upper two panels present the PNe that stay opaque for most of the post-AGB evolution (expansion of the shell starts later and with lower velocity), the bottom two panels concern PNe that become transparent relatively early (expansion starts earlier and with higher velocity). The shaded histograms show the PNLF obtained with a continuous SFH since some 10 Gyr ago until now. The coloured lines show simulations with star formation ending 3, 6 and 9 Gyr ago. Both shaded histograms are supplemented with the observed PNLF outline that combines[29] the bright steep end and the faint tail. At the left side of all panels, the canonical value of M^*_{5007} is indicated as a vertical dashed line with a grey band representing the possible range of this value when correction for extinction is considered (see Supplementary Fig. 1).

torus and thin lobes, 3D modelling[19] reproduces the line emissivities well (including that of [O III]). The details of the evolution and expansion of PNe are still not well understood. Our results puts constraints on this evolution for those PNe that make up the peak of the PNLF.

The brightness and the evolutionary speed of the central stars of PNe, both crucial to the PNLF, are influenced by physical processes in the previous AGB phase, in particular the mass loss and the mixing which bring the products of nuclear burning to the surface. The details of the observed PNLF may put constraints on the efficiency of these still poorly understood processes in AGB stars.

The models give new information about the final fate of the Sun. In our models, it is near the low-mass limit for PN formation. The Sun still reaches a temperature high enough to ionize the ejecta before they disperse. Hydrogen ionization begins 5,000 years after the end of the AGB, and [O III] appears from 12,500 years. The stellar luminosity suffices to put its PN within a magnitude of the bright cut-off of the PNLF. However, at this late time, it is expected that the ejecta will no longer be optically thick, and therefore the PN may be rather fainter than this. If the Sun leaves the AGB during the helium-burning phase of the thermal pulse cycle, its luminosity and speed of evolution will be three times lower and no PN will form. The Sun is close to the lowest-mass star that can still produce a PN.

Methods

La Plata stellar evolution code. LPCODE is a 1D stellar evolution code that has been widely used for the computation of full evolutionary sequences from the zero-age main sequence to the white dwarf stage[20–22]. The last version of LPCODE[14] includes a state-of-the-art treatment of atomic, molecular and conductive opacities[23–25] as well as a detailed treatment of stellar winds and convective boundary mixing. Specifically, LPCODE takes into account both carbon- and oxygen-rich compositions for the determination of both opacity and the stellar wind regime. In addition, convective boundary mixing has been carefully calibrated at different evolutionary stages to reproduce several AGB and post-AGB observables[14]. The post-AGB evolution of the seven tracks computed with this code and discussed in this article are presented in Fig. 1. Each star evolves first at constant luminosity to higher temperatures, followed by a rapid fading and slow cooling. The speed of evolution is much faster at higher stellar mass, so that lower-mass stars spend much longer at their peak luminosity than higher-mass stars do. A metallicity of $Z=0.01$ was selected as being appropriate for Sun-like stars. The post-AGB tracks have little dependence on metallicity, and using $Z=0.02$ would cause only minor changes to the derived masses and ages of the stars. A $1.25M_{\odot}$ track[14] was not used for the interpolations because it was affected by a thermal pulse unusually close to the AGB turn-off which affected the subsequent evolution. The $1M_{\odot}$ presented here was adjusted to ensure that it left the AGB during the hydrogen-burning phase, by briefly turning off the stellar wind until the hydrogen shell had fully activated.

Torun photoionization code. The Torun codes were written in their original form some 20 years ago[15]. The central star is approximated as a black body. The nebula is approximated with a spherically symmetric shell having assumed inner and outer radii and radial density distribution. The chemical composition of the nebular gas was taken from the data set named PLANetary which is included as a part of the Cloudy code[26]. No dust presence was assumed. The ionization state of gas was computed by solving the equations of statistical equilibrium and iterated to convergence with the kinetic temperature and electron density. These codes were not written in a form suitable for public availability but they are easy to adapt to different needs and run very fast on standard workstations. They have been used in numerous publications.

[O III] magnitudes for individual stellar tracks. We first derived [O III] fluxes from a single evolutionary track, for a particular stellar mass. At this step we were interested in maximizing the flux emitted in the [O III] line. The shell parameters were adopted to secure that the PN stays opaque during the whole stellar evolution, the maximum-nebula hypothesis. As the stellar temperature increases and the number of ionizing photons goes up, the ionization front expands and the ionized mass increases. To obtain opaque PNe, the total mass of the shell should exceed the ionized mass. We found that a constant density shell of inner radius of 0.01 pc, outer radius of 0.02 pc and total mass of $0.15M_{\odot}$ fulfils our demands for each of the central star tracks. The resulting hydrogen number density ~1.5×10^5 cm^{-3} guarantees confinement of the ionization front even for the hottest stars. These parameters remain typical for unevolved PNe. For each of the tracks presented in Fig. 1 the flux evolution in the [O III] line was calculated using the Torun model described above. We converted the [O III] line flux to magnitude scale and in this way obtained the dependencies shown in Fig. 2.

We also derived the central star luminosity fraction that is reprocessed into nebular flux in the [O III] 5,007 Å line. The maxima of this reprocessing efficiency remain nearly constant, at the value ~0.12 which is in agreement with earlier modelling[27]. However, the actual values of this efficiency vary considerably with stellar evolution: they first increase with $T_{\rm eff}$, then start to decrease because of higher oxygen ionization and further decrease because the star enters the cooling track. In fact, they closely follow the time dependencies of [O III] 5007 Å fluxes drawn in Fig. 2.

PNLF for expanding PNe in composite stellar populations. To account for simultaneous evolution of the central star and the expansion of nebular shell, we applied a simple scheme. We kept the nebular inner radius fixed and the total nebular mass constant. The shell is assumed to have a constant density with radius. We specified the outer radius as expanding with a constant velocity. The expansion of the outer radius together with a constant inner radius agrees with the observed velocity fields, which have the highest expansion velocities at the outer edge and very low velocity near the inner radius. The expansion results in a fast decrease of the gas density and in consequence of the nebular opacity. The model with expansion starting at the moment when the star leaves the AGB almost immediately becomes transparent. Hydrodynamic calculations[3] show a brief phase of acceleration, caused by the overpressure of the developing ionized region, followed by a plateau. We therefore introduced a delay of the beginning of the (constant) expansion phase. As previously, we want to apply the same shell model to all of the synthetic tracks. Because the evolutionary tracks differ considerably in timescales, we apply the temperature criterion—the nebula starts to expand after the central star effective temperature reaches a specified value. This does not mean that the early phase is static; as the star heats up, the ionization front moves through the opaque shell increasing gradually the nebular ionized radius and the ionized mass. Two parameters define our simplistic models: the threshold temperature which defines the early opaque phase and the expansion velocity which determines the late transparent phase of nebular evolution. As previously, the inner radius equals 0.01 pc while the outer radius initially has the value of 0.02 pc and later expands but not to more than 0.5 pc. The total mass to be ionized was assumed to be $0.1M_{\odot}$, a little lower than at previous computations, as now we are interested in nebulae that at some moment should become transparent. The resulting hydrogen number densities decrease with post-AGB time from ~10^5 cm^{-3} to ~5 cm^{-3}. All these parameters agree with the rather wide limits of physical characteristics that define a PN[28].

By trial and error, we pinpointed two nebular models that represent two representative scenarios. One model is predominantly opaque for all evolutionary tracks: it starts expanding with a velocity of 20 km s^{-1} after the star heats up to 60,000 K. The second model expands a little faster (30 km s^{-1}), and expansion starts somewhat earlier at the temperature of 40,000 K; this model is predominantly transparent for all simulated tracks. These expansion velocities are typical for PNe. The two models are, respectively, the intermediate-nebula and the minimum-nebula hypothesis.

The most massive stellar model ($M_i = 3M_{\odot}$) in both hypotheses evolves so fast that the nebula stays opaque throughout the complete brightest phase and becomes transparent only very late on the cooling track. For the least massive track ($M_i = 1\ M_{\odot}$), the nebula also stays opaque, but for the opposite reason: the temperature evolution is very slow. For the five intermediate evolutionary tracks, the 'opaque period' varies from 600 to 6,000 years for the minimum-nebulae hypothesis, whereas for the intermediate-nebula hypothesis it remains opaque about 50% longer. In both cases, the periods for the nebulae for staying opaque are within reasonable limits.

The carefully computed set of seven tracks (see Fig. 1) served as the base for interpolation on a dense time grid. To interpolate among the tracks, we identified key points corresponding to well-defined post-AGB evolutionary phases. The individual evolutionary tracks were then reduced to the same number of 'equivalent points' between these key points. For a given age, we then computed the expected mass of the post-AGB remnant ($M_f^{\rm synthetic}$) and constructed the interpolated track by interpolating in final mass at equivalent points between the two neighbouring tracks, with masses $M_f^{\rm evol.,A}$ and $M_f^{\rm evol.,B}$ such that $M_f^{\rm evol.,A} < M_f^{\rm synthetic} < M_f^{\rm evol.,B}$. We computed synthetic tracks interpolated to a uniform grid in the age of the stellar population, to every 0.5 Gyr in the range from 0.25 Gyr to 9.75 Gyr. This grid forms the base for assembling simple stellar populations.

To build a histogram, we divided the magnitude axis into 0.5 mag bins (a value comparable with published observed data). The relative time spent by the evolutionary track within given magnitude limits provides a measure of the probability of finding a PN in this bin. We interpolated the evolutionary track to a dense time grid and counted the number of such grid-points within each magnitude bin. A step of 5 yr seems sufficient to obtain an adequate PNLF. The post-AGB evolution slows considerably with decreasing stellar luminosity leading to more numerous faint objects. After some time the PN disperses. We calculate the time spent in each magnitude bin up to our adopted limit of 20,000 years, which is well above the ages that contribute to our histograms and is in agreement with recent PN visibility analysis[3].

Having this data set, we can integrate the PNLF contributions from individual synthetic tracks for each of which the SFH and IMF are used to calculate weighting factors . We simulate a simple, constant SFH started and finished at the given ages. However, the equal steps in stellar age translate to steps dM in initial mass M that are increasing with M. To account for the IMF, we therefore multiplied each individual contribution by the mass step dM and by the Salpeter exponent $M^{-2.35}$ and then summed them up. In this way, the histograms in Fig. 3 were obtained separately for opaque and for transparent shells.

Data availability. The data that support the plots within this paper and other findings of this study are available from the corresponding author upon reasonable request.

Received: 25 April 2017; Accepted: 2 April 2018;
Published online: 07 May 2018

References

1. Vassiliadis, E. & Wood, P. R. Post-asymptotic giant branch evolution of low- to intermediate-mass stars. *Astrophys. J. Suppl. Ser.* **92**, 125–144 (1994).
2. Bloecker, T. Stellar evolution of low- and intermediate-mass stars. II. Post-AGB evolution. *Astron. Astrophys.* **299**, 755–769 (1995).
3. Jacob, R., Schönberner, D. & Steffen, M. The evolution of planetary nebulae. VIII. True expansion rates and visibility times. *Astron. Astrophys.* **558**, A78 (2013).
4. Jacoby, G. H., Ciardullo, R. & Ford, H. C. Planetary nebulae as distance indicators. *Publ. Astron. Soc. Pac.* **4**, 42–56 (1988).
5. Ciardullo, R. The planetary nebula luminosity function at the dawn of Gaia. *Astrophys. Space Sci.* **341**, 151–161 (2012).
6. Ciardullo, R. The planetary nebula luminosity function and its issues. *Proc. IAU* **29B**, 15–19 (2016).
7. Jacoby, G. H. The luminosity function for planetary nebulae and the number of planetary nebulae in local group galaxies. *Astrophys. J. Suppl. Ser.* **42**, 1–18 (1980).
8. Allen, C. W. *Astrophysical Quantities* 3rd edn (ed. Cox, A. N.) (Athlone, London, 1973).
9. Mendez, R. H. & Soffner, T. Improved simulations of the planetary nebula luminosity function. *Astron. Astrophys.* **321**, 898–906 (1997).
10. Méndez, R. H., Teodorescu, A. M., Schönberner, D., Jacob, R. & Steffen, M. Toward better simulations of planetary nebulae luminosity functions. *Astrophys. J.* **681**, 325–332 (2008).
11. Marigo, P., Girardi, L., Weiss, A., Groenewegen, M. A. T. & Chiosi, C. Evolution of planetary nebulae. II. Population effects on the bright cut-off of the PNLF. *Astron. Astrophys.* **423**, 995–1015 (2004).
12. Schönberner, D., Jacob, R., Steffen, M. & Sandin, C. The evolution of planetary nebulae. IV. On the physics of the luminosity function. *Astron. Astrophys.* **473**, 467–484 (2007).
13. Gesicki, K., Zijlstra, A. A., Hajduk, M. & Szyszka, C. Accelerated post-AGB evolution, initial-final mass relations, and the star-formation history of the Galactic bulge. *Astron. Astrophys.* **566**, A48 (2014).
14. Miller Bertolami, M. M. New models for the evolution of post-asymptotic giant branch stars and central stars of planetary nebulae. *Astron. Astrophys.* **588**, A25 (2016).
15. Gesicki, K., Acker, A. & Szczerba, R. Modelling the structure of selected planetary nebulae. *Astron. Astrophys.* **309**, 907–916 (1996).
16. Heavens, A., Panter, B., Jimenez, R. & Dunlop, J. The star-formation history of the Universe from the stellar populations of nearby galaxies. *Nature* **428**, 625–627 (2004).
17. McDermid, R. M. et al. The ATLAS3D Project — XXX. Star formation histories and stellar population scaling relations of early-type galaxies. *Mon. Not. R. Astron. Soc.* **448**, 3484–3513 (2015).
18. Richer, M. G., McCall, M. L. & Arimoto, N. Theoretical models of the planetary nebula populations in galaxies: the ISM oxygen abundance when star formation stops. *Astron. Astrophys. Suppl. Ser.* **122**, 215–233 (1997).
19. Gesicki, K., Zijlstra, A. A. & Morisset, C. 3D pyCloudy modelling of bipolar planetary nebulae: evidence for fast fading of the lobes. *Astron. Astrophys.* **585**, A69 (2016).
20. Miller Bertolami, M. M. & Althaus, L. G. Full evolutionary models for PG 1159 stars. Implications for the helium-rich O(He) stars. *Astron. Astrophys.* **454**, 845–854 (2006).
21. Renedo, I. et al. New cooling sequences for old white dwarfs. *Astrophys. J.* **717**, 183–195 (2010).
22. Althaus, L. G., Miller Bertolami, M. M. & Córsico, A. H. New evolutionary sequences for extremely low-mass white dwarfs. Homogeneous mass and age determinations and asteroseismic prospects. *Astron. Astrophys.* **557**, A19 (2013).
23. Iglesias, C. A. & Rogers, F. J. Updated opal opacities. *Astrophys. J.* **464**, 943–953 (1996).
24. Cassisi, S., Potekhin, A. Y., Pietrinferni, A., Catelan, M. & Salaris, M. Updated electron-conduction opacities: the impact on low-mass stellar models. *Astrophys. J.* **661**, 1094–1104 (2007).
25. Weiss, A. & Ferguson, J. W. New asymptotic giant branch models for a range of metallicities. *Astron. Astrophys.* **508**, 1343–1358 (2009).
26. Ferland, G. J. et al. The 2013 release of Cloudy. *Rev. Mex. Astron. Astr.* **49**, 137–163 (2013).
27. Schönberner, D., Jacob, R., Sandin, C. & Steffen, M. The evolution of planetary nebulae. VII. Modelling planetary nebulae of distant stellar systems. *Astron. Astrophys.* **523**, A86 (2010).
28. Frew, D. J. & Parker, Q. A. Planetary nebulae: observational properties, mimics and diagnostics. *Publ. Astron. Soc. Aust.* **27**, 129–148 (2010).
29. Ciardullo, R., Jacoby, G. H., Ford, H. C. & Neill, J. D. Planetary nebulae as standard candles. II—The calibration in M31 and its companions. *Astrophys. J.* **339**, 53–69 (1989).

Acknowledgements

A.A.Z. and K.G. acknowledge the financial support by The University of Manchester and by Nicolaus Copernicus University. A.A.Z. is supported by the UK Science and Technology Facility Council (STFC) under grant ST/P000649/1. M.M.M.B. is partially suported by ANPCyT and CONICET through grants PICT-2 014-2708 and PIP 112-200801-00940 and also by a Return Fellowship from the Alexander von Humboldt Foundation.

Author contributions

A.A.Z. and K.G. developed the concept. M.M.M.B. provided the post-AGB evolutionary sequences obtained with LPCODE and computed the supplementary data. K.G. adopted the Torun codes for the present work, performed the photoionization calculations and synthesized the PNLF. All authors participated in discussions of the results, in their presentations in figures and descriptions in manuscript and in pinpointing the conclusions.

Competing interests

The authors declare no competing interests.

Additional information

Supplementary information is available for this paper at https://doi.org/10.1038/s41550-018-0453-9.

Reprints and permissions information is available at www.nature.com/reprints.

Correspondence and requests for materials should be addressed to K.G.

Publisher's note: Springer Nature remains neutral with regard to jurisdictional claims in published maps and institutional affiliations.